

Research Article

Dust Concentration Changing Regularities and Dust Reduction Technology by Spray Negative Pressure in Fully Mechanized Mining Face

Lirong Wu ^{1,2} Hongxuan Chen ¹ Jiamin Li ¹ Shican Fu,¹ and Yuyan Zhuang¹

¹College of Safety and Environmental Engineering, Shandong University of Science and Technology, Qingdao 266590, China

²State Key Laboratory of Mining Disaster Prevention and Control co-Founded by Shandong Province and the Ministry of Science and Technology, Shandong University of Science and Technology, Qingdao 266590, China

Correspondence should be addressed to Jiamin Li; lijiamin980328@126.com

Received 27 June 2021; Accepted 13 August 2021; Published 1 October 2021

Academic Editor: Chenhao Sun

Copyright © 2021 Lirong Wu et al. This is an open access article distributed under the Creative Commons Attribution License, which permits unrestricted use, distribution, and reproduction in any medium, provided the original work is properly cited.

The dust concentration changing regularities are the basis to take dust depression measures, which is greatly influenced by the airflow. In the software of FLUENT, the value of ventilation velocity is set as a constant, which cannot express the real ventilation. According to the flow characteristics of the sublayer and data from Nicholas' experiment, the ventilation velocity distribution formula of sublayer in the inlet section of fully mechanized caving coal face is deduced. The boundary condition of velocity is given by UDF. Taking the 3^{top1110} fully mechanized caving coal face as an example, the dust distribution in the process of coal mining and hydraulic support shifting was studied. According to the dust-spray coupling experiment, three types of nozzle are chosen based on the efficiency of dust suppression. Combining the dust migration rule and the characteristics of nozzles, the negative pressure-secondary dust suppression devices of spray were developed and applied. And the above measures have lowered the dust concentration effectively.

1. Introduction

High-concentration dust has been an issue that impedes the safe and efficient coal mining in fully mechanized mining faces. Coal dust is one of the five major disasters in coal mines, which can not only lead to dust and gas explosion accidents but also cause workers' pneumoconiosis. According to the notification by the National Health and Family Planning Commission of PRC, the cumulative number of occupational disease cases in China was as high as 951359 by 2017, of which 853847 were pneumoconiosis cases, accounting for 89.8% of the total occupational disease cases in China. It is predicted that the pneumoconiosis cases in China will keep rising in the coming 10-15 years [1, 2].

In order to control the dust effectively, making clear the coal dust concentration changeable rule is the basis. And much research had been done by numerical simulation. Lai [3] used the finite volume method of computational fluid dynamics to solve the problem and compiled a computer

program to simulate the distribution of wind speed and dust concentration in the three-dimensional space of fully mechanized working face. Nakayama et al. [4], Patankar and Joseph [5], and Yu et al. [6] used a large eddy simulation (LES) method to simulate gas movement, and the Eulerian Lagrangian method was used to simulate dust particle movement. According to the two basic flow field types of plane wake flow and turbulent jet, the spatial distribution characteristics of dust particles with different Stokes (st) numbers were numerically simulated. Housiadas et al. [7] and Wang et al. [8] studied the air flow field and dust concentration distribution law of the extraction type local ventilation mode in the heading face. Liu et al. [9] and Niu et al. [10] carried out numerical simulation on the dust movement law of working flour by using computational fluid dynamics FLUENT software. Zhou et al. [11, 12], Wu [13], and Sun et al. [14] studied the dust movement law of multiple dust sources in a fully mechanized caving face and the influencing factors of dust concentration. Yao et al. [15] studied the influence of

different parameters on the dust flow law of a fully mechanized caving face and the dust generation law of different working procedures in steeply inclined fully mechanized caving face. Ren et al. [16] focused on airflow and coal dust dynamics at the intersection between the fully mechanized caving face and the air intake lane and proposed an optimal layout of air curtain at the entrance of air intake lane and working face based on the results of numerical simulation.

The application of spray technology in fully mechanized coal caving workplace is aimed at reducing the coal dust concentration. Since 1980s, all kinds of dust removal technologies have been developed, and the theory of spray and dust suppression has been continuously improved [17]. At present, most of the coal faces use spray dust control technology to prevent dust, and in most cases, high pressure is taken to improve dust removal efficiency. High-pressure spray dust suppression technology is applied earlier in the United States, the former Soviet Union, Germany, and other countries [18, 19]. The dust reduction efficiency of the shearer driver was 94%. Although high-pressure spray can improve the efficiency of dust fall, high-pressure spray will cause dust disturbance, resulting in secondary dust. Therefore, nozzle installation location, spray pressure, and flow rate need to be adjusted. A large number of experiments and studies have been carried out by the US Mining Bureau, and a new type of external spray cleaning device for Drum Shearers has been developed, which makes the dust laden airflow and fresh air flow run separately and overcomes the eddy current effect produced by the external spray system in adverse wind spray [20]. Liu [21] used LS-2000 split type laser atomization droplet size analyzer to measure the droplet size, distribution, and velocity of different swirl water mist nozzles and obtained the optimal structural parameters of the medium and low-pressure single fluid through swirl atomizing nozzle. Wang et al. [22] used the three-dimensional LDV/APV system to measure the three-dimensional velocity of the spray field of the dust suppression nozzle accurately. The experimental results show that with the increase of the nozzle set fluid pressure, the fog particle size gradually decreases, the radial coverage of the fog field expands, and the volume flux of the dusty air increases gradually. Zhou et al. [23] designed a nozzle atomization experimental system by using Winner313 laser particle size analyzer. The atomizing particle size of the common nozzles in the coal mining face was measured, and it was determined that the spray particle size distribution at 8 MPa had the best effect on the dust reduction in the coal mining face. Peng et al. [24] added a fan to the shearer's spray device to develop an air-assisted PM10 control device, in combination with the airflow-carrying-droplet mechanism. Wang et al. [25, 26] had done the experimental study on dust reduction via spray using a surfactant solution.

In order to control the coal dust concentration in the fully mechanized mining face more effectively, this paper first deduced ventilation velocity distribution formula of base course in inlet section and wrote the inlet velocity programs (UDF), which was interpreted in FLUENT, replacing the constant value set as usual. Then, the ventilation velocity set in the numerical simulation can express the real condi-

tion and does the dust concentration changeable rule. Based on the nozzle jet characteristic experiment and spray dust fall experiment, the preferable nozzles have been selected. Combining the dust production regulation and nozzle characteristics, the negative pressure resecondary dust suppression device is used, which has two effects. First, the proper nozzles have been chosen and set in the dust suppression device. Based on the dust migration rule, the spray direction of nozzles is adjusted. Then, the dust produced in the process of coal mining can be depressed to a great extent. Second, in order to catch the dust, the negative pressure resecondary dust suppression theory is used in the device. Based on the above, the dust can be controlled effectively.

2. Methods

2.1. Theoretical Study of Dust Migration Rule. In fully mechanized mining faces, the gas flow control equations apply the three dimensional steady incompressible Navier-Stokes equation. The turbulent flow model uses the $k-\varepsilon$ double equation model. The momentum transfer is considered, and the heat passage is neglected.

Continuous equation:

$$\frac{\partial}{\partial x_i}(\rho u_i) = 0. \quad (1)$$

Equation of motion:

$$\frac{\partial c}{\partial x_i}(\rho u_i u_j) = -\frac{\partial p}{\partial x_i} + \frac{\partial}{\partial x_i} \left[(\mu + \mu_t) \left(\frac{\partial u_j}{\partial x_i} + \frac{\partial u_i}{\partial x_j} \right) \right] \quad (2)$$

k equation:

$$\frac{\partial}{\partial x_i}(\rho u_i k) = \frac{\partial}{\partial x_i} \left[\left(\mu + \frac{\mu_t}{\sigma_k} \right) \frac{\partial k}{\partial x_i} \right] + G_k - \rho \varepsilon. \quad (3)$$

ε equation:

$$\begin{aligned} \frac{\partial}{\partial x_i}(\rho u_i \varepsilon) &= \frac{\partial}{\partial x_i} \left[\left(\mu + \frac{\mu_t}{\sigma_\varepsilon} \right) \frac{\partial \varepsilon}{\partial x_i} \right] + \frac{C_{\varepsilon 1} \varepsilon}{k} G_k \varepsilon^2 - C_{\varepsilon 2} \rho \frac{\varepsilon^2}{k}, \\ \mu_t &= C_{\mu} \rho \frac{k^2}{\varepsilon}, \\ G_K &= \mu_t \frac{\partial u_j}{\partial x_i} \left(\frac{\partial u_j}{\partial x_i} + \frac{\partial u_i}{\partial x_j} \right), \end{aligned} \quad (4)$$

where G_K is the turbulent kinetic energy change rate generated by shear force changes; k is the turbulent kinetic energy, m^2/s^2 ; ε is the turbulent dissipation rate, m^2/s^3 ; μ is the laminar viscous coefficient, Pa·s; μ_t is the turbulent viscosity coefficient, Pa·s; p is the the turbulence of effective pressure, Pa; ρ is the gas density, kg/m^3 ; x_i is the coordinate in the direction of x , y , and z , m; μ_t is the ventilation of fluid

in the direction of x , y , and z , m/s; $C_{\varepsilon 1}$, $C_{\varepsilon 2}$, C_{μ} , σ_{ε} , and σ_k are the constant, taking 1.44, 1.92, 0.09, 1.3, and 1.0 successively.

The particle motion equation is solved by the integral operation in discrete time steps. And the movement track is as follows:

$$\frac{dx}{dt} = u_p. \quad (5)$$

2.2. Theoretical Analysis of Ventilation Velocity Distribution at Entrance Section. The ventilation velocity distribution in the fully mechanized mining coal face affects the dust migration rule. According to the different Reynolds numbers, the fluid flow can be divided into the laminar flow and turbulent flow.

For the cylindrical space, when the fluid flow state is laminar, the velocity distribution law of the section is a rotating paraboloid. When the fluid flow state is turbulent, as its flow mechanism is different from laminar flow, its velocity distribution is fundamentally different from that of laminar flow. In most areas near the pipe axis, the transverse pulsation of fluid particles makes the momentum exchange between the flow layers more intense, which becomes the turbulent core area. The pulsation of the laminar flow thin layer near the wall disappears due to wall restriction. At the same time, the viscous force between the laminar flow layers makes the velocity drop sharply and the velocity gradient is large. This thin layer is called the viscous bottom layer. According to the Prandtl hypothesis and Nicholas experiment, the velocity distribution function of the viscous bottom layer and turbulent core area in cylindrical space section can be obtained.

The velocity distribution formula of the entrance section of the fully mechanized caving coal face should adopt the noncylindrical space velocity distribution formula. For noncylindrical spaces, in the early 1950s, B-H-Voronin (Soviet Union mine ventilation scientist) published the velocity distribution function on the cross-section of the roadway. In 1977, the ventilation safety department of Northeast Institute of technology revised the formula deduced by B-H Voronin on the basis of experimental research. In 1982, Ji Chaosong (Professor of Beijing Institute of iron and steel) theoretically deduced the distribution function of tunnel wind speed which is different from that derived by B-H Voronin. In 1989, Yu Yuejin analyzed the defects of the formula on the basis of the above research and put forward the L-Prandtl formula of the velocity distribution in the roadway according to the Prandtl hypothesis. The above formula does not distinguish the difference of velocity between the viscous bottom and turbulent core. Based on the above research, the velocity distribution formula of the noncylindrical space viscous bottom is derived in this paper [27].

In the viscous bottom layer, the velocity distribution can be approximately considered a straight line distribution, that is,

$$\frac{dv_x}{dy} = \frac{v_x}{y}. \quad (6)$$

The stress can be approximately expressed as follows:

$$\tau = \mu \frac{v_x}{y}, \quad y \leq \delta, \quad (7)$$

where δ is the thickness of the viscous bottom layer. It can be obtained from formula (7):

$$v_x = v_*^2 \frac{y}{\nu}. \quad (8)$$

Let

$$v_* = \sqrt{\frac{\tau}{\rho}}. \quad (9)$$

In formula (9), v_* is the resistance velocity. According to Bernoulli's equation and Darcy's law, the following formula can be deduced:

$$v_* = \bar{v} \sqrt{\frac{\lambda}{8}} = \bar{v} \frac{\sqrt{\alpha}}{\rho}, \quad (10)$$

where λ is the Darcy coefficient, dimensionless and α is the friction coefficient, kg/m^3 .

According to the Nikolaz experiment, the following formula is satisfied in the laminar flow region:

$$\lambda = \frac{64}{Re} = \frac{64\nu}{v_x d}, \quad (11)$$

where d is the equivalent diameter, m.

Formulas (10) and (11) are substituted into formula (8), and the velocity distribution formula of the viscous bottom zone expressed by \bar{v} ; r/r_0 is as follows:

$$v_x = \bar{v} \sqrt{2 \left(1 - \frac{r}{r_0}\right)}. \quad (12)$$

L-Prandtl's two hypotheses are as follows:

- (1) The turbulent shear stress is constant along the section and equal to the wall shear stress τ
- (2) There is a linear relationship between the mixing length l and the distance y to the cylinder wall, i.e., $l = ky$

For the turbulent region, according to Prandtl's above hypothesis, there is

$$\tau = \rho k^2 y^2 \left(\frac{dv_x}{dy}\right)^2. \quad (13)$$

It can be obtained from formulas (9) and (13):

$$\frac{dv_x}{dy} = \frac{v_*}{ky}. \quad (14)$$

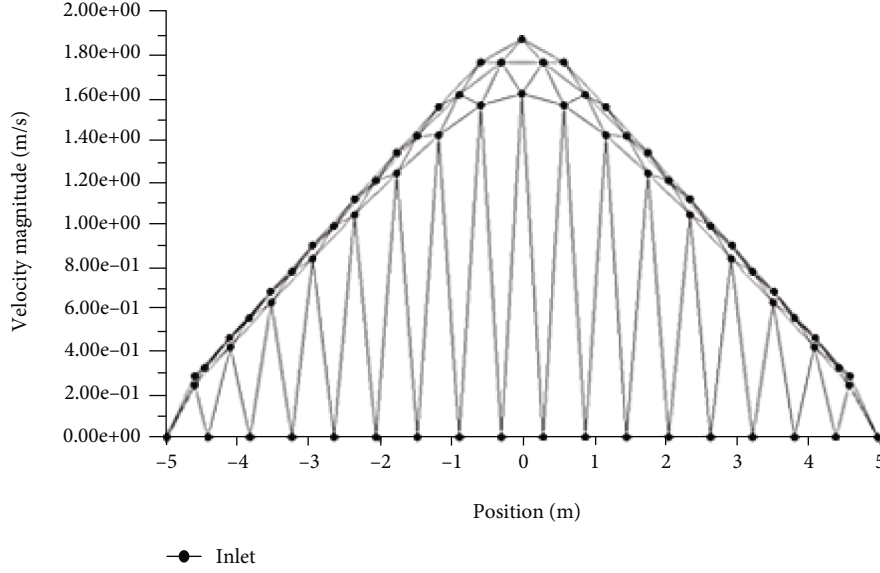


FIGURE 1: The ventilation in the entry section at the x -axis.

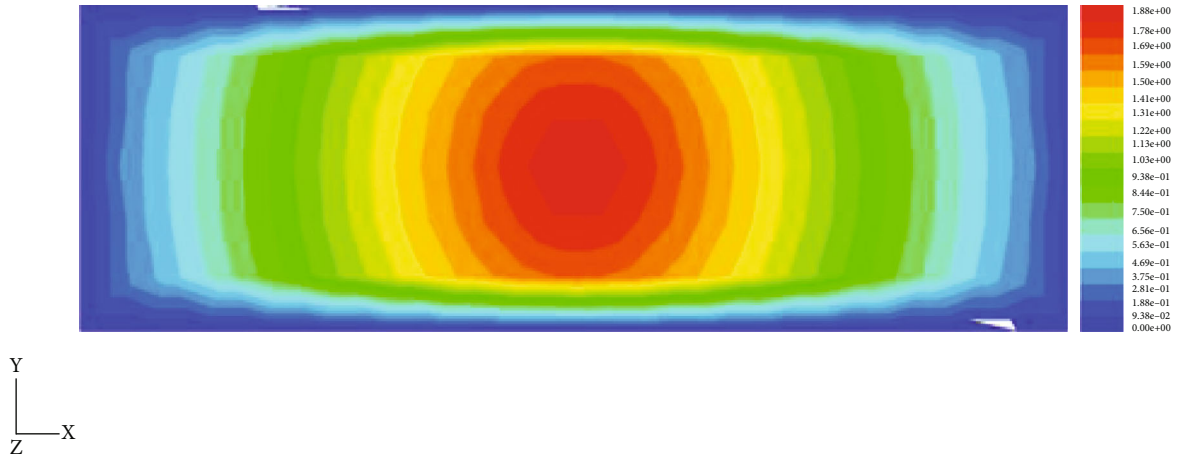


FIGURE 2: The ventilation in the entry section at the x -axis.

By integrating formula (14), the following can be obtained:

$$v_x = \frac{1}{k} v_* \ln y + C. \quad (15)$$

Assuming that the velocity at the boundary between the viscous bottom and turbulent flow is expressed by v_b , then, the boundary condition is $y = \phi \varepsilon$, $v_x = v_b$. Substituting the boundary condition into formula (15), the following results can be obtained:

$$C = v_b - \frac{1}{k} v_* \ln \phi \varepsilon, \quad (16)$$

where ϕ is the shape coefficient determined by the roughness of the cylinder wall and ε is the absolute roughness of the pipe wall.

Substituting formula (16) into (15), then,

$$v_x = \frac{1}{k} v_* \ln \frac{y}{\phi \varepsilon} + v_b. \quad (17)$$

Let $C_2 = (v_b/v_*) - (1/k) \ln \phi$, then,

$$\frac{v_x}{v_*} = \frac{1}{k} \ln \frac{y}{\varepsilon} + C_2. \quad (18)$$

According to the Nicholas experiment curve, $k = 0.40$, and $C_2 = 8.48$, then, the results are as follows:

$$\frac{v_x}{v_*} = 2.5 \ln \frac{y}{\varepsilon} + 8.48. \quad (19)$$

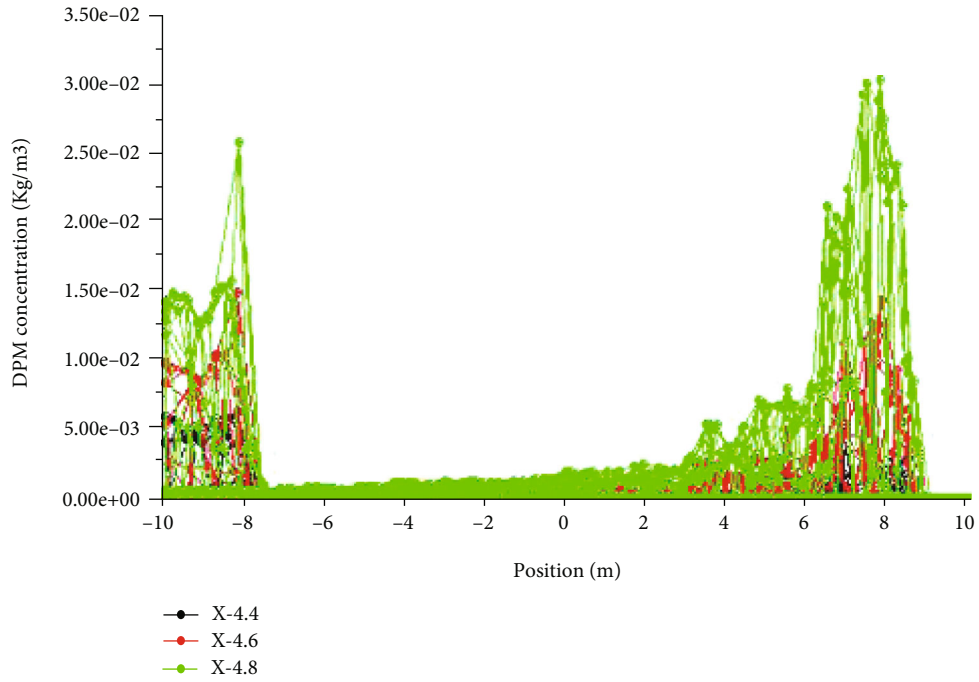


FIGURE 3: Variation chart of dust concentration in different sections of coal mining operation.

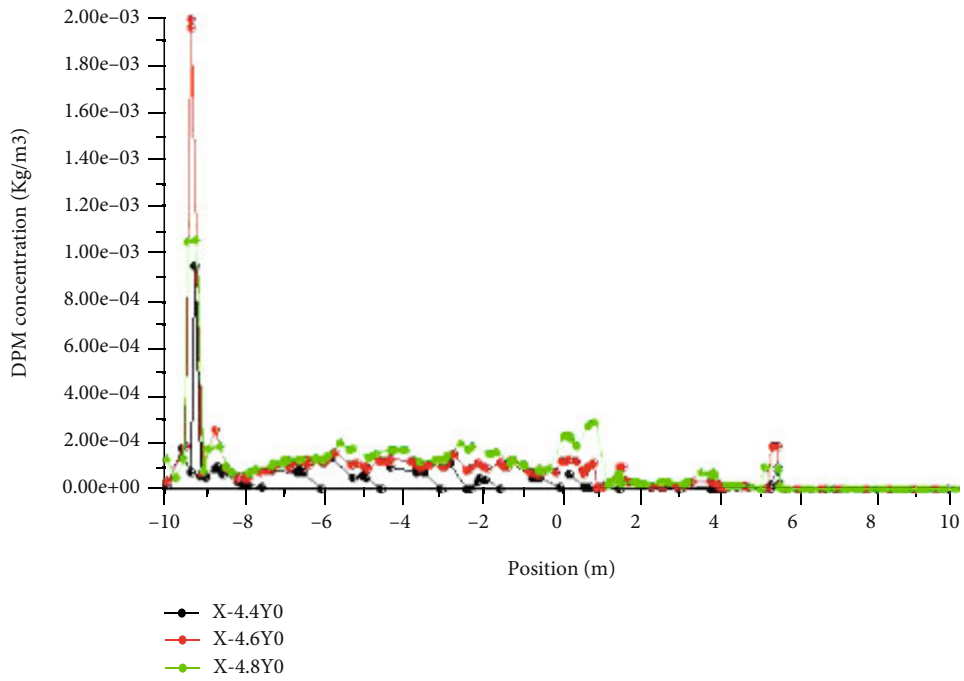


FIGURE 4: Variation chart of dust concentration in coal mining operation.

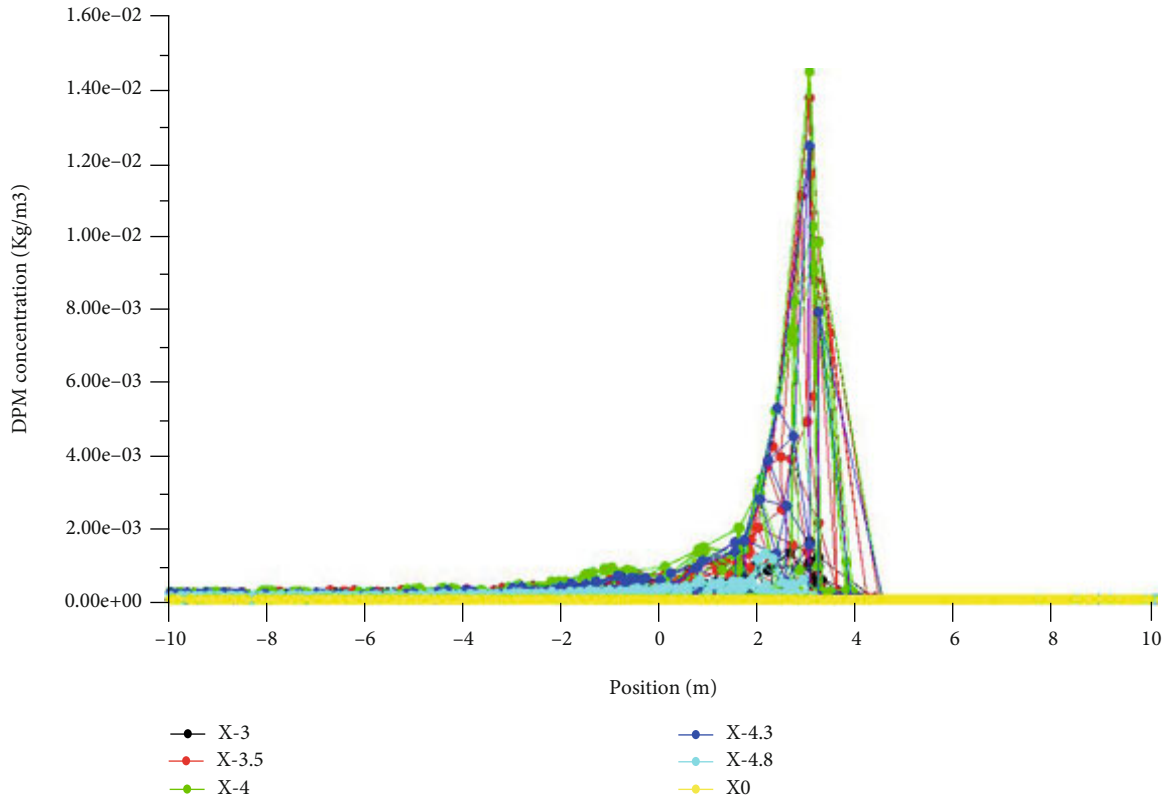


FIGURE 5: Variation chart of dust concentration in support shifting operation.

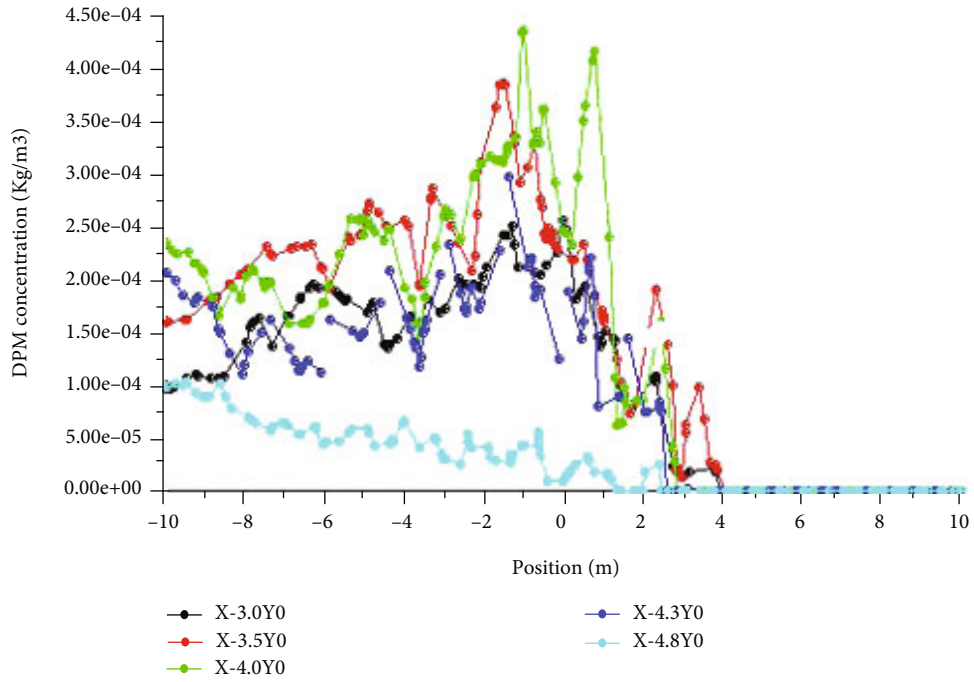







FIGURE 6: Variation chart of dust concentration in support shifting operation.

TABLE 1: Nozzles used in atomization characteristic experiment.

Type	No.	Orifice diameter (mm)	Fog flow shape	Atomization type	Physical picture
A	1#	1.1	Sector	Cone-shaped guide groove direct type	
	2#	1.4			
	3#	1.6			
B	4#	1.6	Solid cone	Mixed type with X-shaped guide core	
	5#	2.0			
	6#	2.4			
C	7#	1.2	Hollow cone	Side guide hole centrifugal	
	8#	1.6			
	9#	2.0			
D	10#	2.4	Square solid cone	Hybrid type with cross opening and X-shaped guide core	
	11#	1.6			
	12#	1.9			
E	13#	2.4	Solid cone	Mixed type with X-shaped guide core	
	14#	2.3			
	15#	2.8			
	16#	3.2			

According to the Nicholas experiment curve, the relationship between $k - \varepsilon$ and ε is as follows:

$$\varepsilon = 7.4r_0 10^{1/-2\sqrt{\lambda}}. \quad (20)$$

By substituting formulas (9) and (20) into (19), $\rho = 1.2 \text{ kg/m}^3$ is set, and the velocity distribution formula of turbulent area expressed by \bar{v} and $\alpha; r/r_0$ is as follows:

$$v_x = \bar{v} \left[1 + 3.17\sqrt{\alpha} + 2.28\sqrt{\alpha} \ln \left(1 - \frac{r}{r_0} \right) \right]. \quad (21)$$

Formulas (12) and (21) are the velocity distribution formulas of the viscous bottom layer and turbulent area of a noncircular pipe, respectively. The section of the fully mechanized caving coal face can be regarded as a kind of noncircular pipe, so formulas (12) and (21) are also applicable to the distribution of wind speed at the entrance section of the fully mechanized coal caving face.

3. The Simulation of Dust Concentration in Fully Mechanized Mining Workface

Taking the 3^{top1110} work face in the Gao Zhuang Coal Mine as the research object, the dust concentration changing reg-

ularities are simulated by the software of FLUENT. Based on the actual situation of 3^{top1110} working face, the rectangular region is made with the length, width, and height of 20.0 m, 10.0 m, and 3.0 m, respectively. The parameters and boundary conditions of numerical simulation are determined, in which the value of the inlet velocity magnitude is set by UDF(velocity_inlet).

In the standard FLUENT module, the entrance velocity can only be given as a constant value, but in reality, the velocity is a variable on the workface section. User-defined function (UDF) can be used to define the entrance velocity at different positions on the entry face, so as to better calculate the velocity field inside the workface. And the simulation results can better reflect the actual situation of the fully mechanized mining face.

According to the velocity distribution theory at the entrance section of the fully mechanized mining face, the flow state of air flow in workface determines the distribution of velocity. Therefore, the flow state of 3^{top1110} workface in the Gao Zhuang Coal Mine should be identified firstly. When the average velocity of workface is 2 m/s, the Reynolds number is calculated as follows:

$$\text{Re} = \frac{vd}{\nu} = \frac{2.4S/C}{\nu} = \frac{2.4 \cdot 30/26}{14.8 \cdot 10^{-6}} = 623700. \quad (22)$$



(a) Simulation tunnel



(b) Doppler laser beam and data acquisition system

FIGURE 7: Closed experiment box.

It can be seen that the flow state of the workface is turbulent.

According to the velocity distribution formula at the entrance section of the fully mechanized mining face and the actual situation 3^{top1110} workface, the UDF velocity of inlet velocity magnitude (m/s) is compiled by using C language_Let.

User-defined function UDF velocity inlet is interpreted in FLUENT software and set as the boundary condition of velocity at the entrance section of the fully mechanized mining face. The variation of velocity along the x -axis direction of the entrance section is shown in Figure 1. The velocity distribution at the entrance section is shown in Figure 2.

From Figures 1 and 2, it can be seen that the velocity of the workface wall is zero, and the velocity increases from the wall to the core. In the core point the velocity reaches the maximum. The distribution curve of velocity along the x -axis direction of the entrance section approximates a parabola.

When the dust produced by the shearer cutting coal is considered separately, the dust source is the front and rear drums of the shearer. When the average velocity is 2 m/s, the dust concentration on the face 0.2 m, 0.4 m, and 0.6 m away from the coal wall is displayed in Figure 3. The dust concentration on the line 0.2 m, 0.4 m, and 0.6 m away from the coal wall and 1.5 m above the ground is shown in Figure 4.

When the dust produced by hydraulic support moving operation is considered separately, the average wind speed

at the inlet of 2 m/s and the dust source as a line source are set, which is located at the top of the second hydraulic support at the air inlet, close to the edge of the coal outlet ($-4.3 < x < 0.7, z = 2.9$). Assuming that 20 particles are randomly generated at the dust source, the dust concentration distribution at 0.2 m, 0.7 m, 1 m, 1.5 m, 2 m, and 5 m away from the coal wall is shown in Figure 5. The dust concentration distribution along the z -axis direction at the distance of 0.2 m, 0.7 m, 1 m, 1.5 m, 2 m, and 5 m away from the coal wall and 1.5 m above the ground is shown in Figure 6.

4. Experiment on Characteristics of Nozzles and Spray Dust Fall

4.1. Experiment on Atomization Characteristics of Nozzle. In order to optimize the nozzles suitable for spraying and dust fall in the fully mechanized mining face, 5 types of stainless steel nozzles (expressed separately by A–E) including 16 kinds of stainless steel nozzles (1#–16#, respectively) are collected, the traits of which are shown in Table 1. The experiments on atomization characteristics and spray dust fall are completed in the simulation tunnel, which are shown in Figures 7(a) and 7(b). The conventional performance parameters of A–E (1#–16#) nozzles are researched and the conventional performance parameters of A–E (1#–16#) nozzles can be seen in Table 2).

Based on the atomization angle, effective range, and flow of the nozzles, considering the shape and droplet density of the fog flow field observed in the field, 8 kinds of nozzles

TABLE 2: Measurement data of conventional performance parameters of 1#–16# nozzles under different pressures.

Type	No.	Pressure (MPa)	Atomization angle (°)	Effective range (m)	Flow (L/min)	Type	No.	Pressure (MPa)	Atomization angle (°)	Effective range (m)	Flow (L/min)
A	1#	2	111.7	1.0	3.45	C	9#	2	97.8	2.1	3.41
		4	111.2	1.6	4.12			4	90.3	3.3	4.43
		6	110.8	2.4	5.13			6	83.1	3.7	5.49
		8	110.5	3.7	5.86			8	75.7	4.2	6.67
	2#	2	125.1	1.8	3.92		10#	2	96.5	2.5	4.63
		4	123.6	3.2	5.53			4	91.9	3.5	6.13
		6	122.0	3.7	7.13			6	85.3	4.2	7.31
		8	121.9	4.3	7.67			8	76.0	4.3	7.83
	3#	2	99.5	2.0	4.36		11#	2	80.1	2.3	3.67
		4	99.1	2.8	5.98			4	71.6	3.3	4.83
		6	99.0	3.5	7.16			6	71.0	4.1	5.89
		8	98.9	5.2	8.51			8	69.3	4.7	6.83
4#	2	67.7	3.2	4.07	D	12#	2	75.4	3.3	4.42	
	4	65.2	3.9	5.75			4	73.1	3.8	5.60	
	6	62.6	5.0	6.81			6	68.7	4.7	7.29	
	8	59.1	5.1	7.66			8	68.4	5.2	8.72	
B	5#	2	69.8	3.3	4.63	13#	2	71.7	3.3	6.20	
		4	59.3	4.3	6.13		4	66.6	4.3	8.19	
		6	56.2	4.8	7.72		6	65.5	5.1	10.27	
		8	55.5	5.2	9.13		8	61.8	6.1	11.71	
6#	2	72.1	3.5	6.86	14#	2	91.4	2.5	3.77		
	4	61.6	4.5	9.00		4	87.6	3.4	5.14		
	6	59.9	5.2	10.76		6	79.4	4.5	6.28		
	8	59.3	5.7	12.54		8	73.5	5.3	7.05		
7#	2	94.5	1.2	1.29	E	15#	2	80.6	3.8	7.39	
	4	84.5	1.7	1.57			4	67.6	4.6	10.23	
	6	82.9	2.3	2.14			6	65.2	4.9	12.38	
	8	75.8	2.7	2.63			8	62.5	6.5	14.76	
C	8#	2	90.0	1.2	2.29	16#	2	81.4	4.0	10.32	
		4	88.3	1.9	2.85		4	75.5	5.2	13.73	
		6	83.6	2.8	3.43		6	67.0	7.2	16.96	
		8	81.5	3.0	3.94		8	65.9	7.8	19.89	

were selected from 16 kinds of nozzles, including 2# and 3# nozzles in type A, 4# and 5# nozzles in type B, 9# nozzles in type C, 11# and 12# nozzles in type D, and 14# nozzles in type E nozzles. In order to be different from the number of nozzles in conventional parameter measurement, in the atomization characteristic test, according to the order of 8 kinds of nozzles in 16 kinds of nozzles, they are numbered as nozzle 1 to nozzle 8, respectively.

According to the experimental results of the nozzle jet characteristics (atomization characteristic parameter table of the experimental nozzle under different pressures can be seen in Tables 3–6), with the increase of spray pressure, the $D_{0.1}$, $D_{0.5}$, $D_{0.9}$, D_{32} , and D_{43} particle sizes of 8 nozzles decreased. The smaller the nozzle droplet diameter, the better the atomizing effect of nozzles, and the stronger

the ability to capture respirable dust. Considering spray equipment can tolerate 8 MPa water pressure, the water pressure of 8 MPa is adopted, under which each nozzle droplet diameter can reach the minimum in experiment. In experiment, nozzle 8 has the best atomization effect. The percentage of respirable dust being captured of 8 nozzles under the water pressure of 8 MPa is shown in Table 7. The routine atomization parameters are summarized in Table 8.

4.2. Spray Dust Fall Experiment. To test the dust reduction effectiveness of nozzles, the spray dust fall experiment was done with the water pressure of 8 MPa and fan speed of 300r/min. The coal dust samples with different particle sizes were prepared. In the experiment, the particle size and

TABLE 3: Atomization characteristic parameter table of nozzles under 2 MPa pressure.

No.	$D_{0.1}$ (μm)	$D_{0.5}$ (μm)	$D_{0.9}$ (μm)	D_{32} (μm)	D_{43} (μm)
1	28.833	65.546	113.142	53.363	68.985
2	25.716	54.966	86.534	45.485	56.285
3	48.874	86.483	132.942	75.410	89.000
4	51.577	93.528	145.390	80.718	96.097
5	33.047	73.819	127.594	58.829	78.308
6	24.844	53.743	85.320	44.235	55.053
7	26.609	55.939	87.507	46.458	57.278
8	23.917	53.212	84.784	43.759	54.539

TABLE 4: Atomization characteristic parameter table of nozzles under 4 MPa pressure.

No.	$D_{0.1}$ (μm)	$D_{0.5}$ (μm)	$D_{0.9}$ (μm)	D_{32} (μm)	D_{43} (μm)
1	23.658	53.669	90.793	43.633	56.344
2	24.066	50.636	82.936	42.703	52.668
3	42.843	77.647	124.600	66.840	80.353
4	51.627	86.723	135.630	72.746	89.276
5	25.109	54.049	87.664	44.546	55.444
6	22.426	49.404	81.704	41.471	51.436
7	24.645	51.669	83.909	43.986	53.651
8	21.902	48.869	81.159	40.957	50.942

TABLE 5: Atomization characteristic parameter table of nozzles under 6 MPa pressure.

No.	$D_{0.1}$ (μm)	$D_{0.5}$ (μm)	$D_{0.9}$ (μm)	D_{32} (μm)	D_{43} (μm)
1	21.034	46.394	75.532	37.782	47.737
2	22.108	45.713	74.358	36.810	47.160
3	39.360	69.499	107.095	59.635	72.266
4	41.084	70.803	114.184	62.172	74.025
5	23.118	47.626	81.559	40.272	50.267
6	20.532	44.457	70.674	36.978	45.721
7	21.660	47.451	73.998	37.042	47.054
8	20.015	43.935	70.274	36.656	45.139

TABLE 6: Atomization characteristic parameter table of nozzles under 8 MPa pressure.

No.	$D_{0.1}$ (μm)	$D_{0.5}$ (μm)	$D_{0.9}$ (μm)	D_{32} (μm)	D_{43} (μm)
1	19.621	41.353	72.306	34.982	44.372
2	19.672	40.022	65.718	34.770	41.933
3	33.075	63.474	105.248	55.575	71.094
4	35.159	62.507	97.962	54.554	63.796
5	22.597	45.320	75.432	38.846	47.944
6	18.804	39.043	62.833	34.393	41.644
7	20.586	40.581	64.996	35.781	42.892
8	18.342	38.541	62.321	33.951	41.162

distribution of coal dust were analyzed by using Doppler laser interferometer (PDI200MD), and the dust concentration was measured by AKFC-92A dust sampler. And 8 kinds of nozzle spray dust fall efficiency are shown in Table 9.

4.3. Research on Spray Dust Fall Devices of Negative Pressure

4.3.1. Theory of Spray Dust Fall with Negative Pressure

(1) *Water Mist Piston Mechanism.* When the nozzle is sprayed outwards, the water mist is formed when the diffusing diameter of the water mist is equal to or larger than the inner diameter of the nozzle. The air inside the nozzle is pushed out by the water mist, and then, the vacuum is formed, thus forming negative pressure. Under the negative pressure, the dust laden airflow can enter the nozzle of the spray device through the suction part.

In the nozzle, the dust in the dusty air flow is repeatedly impacted by the water mist, combined with the water mist, ejected from the pipe, and settles due to the loss of suspension capacity in the air. At the same time, the mixture composed of purified air and water mist continues to be ejected at high speed by the nozzle, forming a negative pressure field at the ejection end, sucking the surrounding dusty air flow into the jet, so that the dust in the air flow can be further washed.

(2) *Entrainment Mechanism of Water Jet.* When the high-speed fog and air flow are ejected, there is a discontinuity with the air flow in the workface. Due to the inevitable interference, the discontinuity loses its stability and generates a vortex. The vortex sucks the surrounding dusty gas into the jet, continuously moves, deforms, and splits to produce turbulence. Its influence gradually develops to the inner and outer sides, forming two free turbulent mixing layers inside and outside. Due to the transverse transmission of momentum, the entrained dusty gas obtains momentum flows forward with the originally emitted fog and air flow, so that the dust in the air flow can collide with the droplets to achieve the purpose of dust reduction. At the same time, the atomized droplets in the jet lose momentum, reduce the velocity, form a certain velocity gradient in the mixing layer, and appear as shear stress. As a result of entrainment and mixing, the jet section expands continuously, while the flow velocity decreases continuously.

4.3.2. *Spray Dust Fall Device of Negative Pressure in Coal Mining Operation.* Combining dust migration rules in coal mining operation and characteristics of nozzles, the spray dust fall device of negative pressures in coal mining operation have been researched, which are shown in Figures 8(a) and 8(b).

The dust control device of negative pressure for coal mining operation is shown in Figure 8(a). It is composed of 4 nozzles and 16 suction ports distributed on the side part. The device is mainly used for reducing the dust generated at the drum and moving along the transverse section of the fully mechanized top coal caving face. The layout of the three spray dust fall devices in coal mining operations is

TABLE 7: The percentage of respirable dust being captured of 8 nozzles under the water pressure of 8 MPa.

Nozzle parameter	1	2	3	4	5	6	7	8
Percentage (%)	84.51	90.73	62.95	62.02	77.11	91.13	86.44	91.36

TABLE 8: The routine atomization parameters of 8 nozzles under the water pressure of 8 MPa.

Nozzle Parameter	1	2	3	4	5	6	7	8
Spray angle (°)	121.8	98.9	59.1	55.5	75.8	69.2	68.3	73.6
Effective range (m)	4.4	5.3	5.2	5.3	4.3	4.7	5.2	5.3
Flow (L/min)	7.66	8.50	7.66	9.12	6.67	6.86	8.75	7.07

TABLE 9: The spray dust removal efficiency with the pressure of 8 MPa and fan rotate speed of 300 r/min.

Nozzle number	Dust removal rate (%)	
	Total dust	Respirable dust
Nozzle 1	42.71	35.87
Nozzle 2	39.21	32.39
Nozzle 3	50.37	46.61
Nozzle 4	47.32	41.71
Nozzle 5	56.30	51.21
Nozzle 6	63.56	59.78
Nozzle 7	60.72	56.17
Nozzle 8	65.82	61.70

shown in Figure 8(b). They are located on the upper, middle, and bottom of the shearer arm.

In order to control the dust concentration effectively, the type of nozzles should be chosen on the basis of the dust migration rule and the characteristics of nozzles. From Figures 3 and 4, in the process of coal mining, under the action of gravity, wind flow, and collision between dusts, it not only exists the transverse diffusion in the workplace but also the longitudinal diffusion to the outlet under the action of wind flow. It is mainly vertical diffusion, and the transverse diffusion range is limited. In the experiments on characteristics of nozzles and spray dust fall, three kinds of nozzles are optimized. Nozzle 5 has a small flow, large atomization angle, and small range. The atomization angles of nozzle 6 and nozzle 8 are less than nozzle 5, and the range and flow are greater than nozzle 5.

The concentration of the dust near the shearer drum is larger, and the granularity is larger. The spray direction of the nozzles located on the upper and bottom of the shearer arm points to the direction of the coal seam. Combining the dust migration rule with the characteristics of nozzles, the nozzle types in the upper dust fall device are nozzle 8, nozzle 8, nozzle 5 and nozzle 5, respectively, and in the bottom part, the nozzle types from left to right are nozzle 5, nozzle 5, nozzle 5 and nozzle 5. The spray direction of the nozzles located on the middle of the shearer arm is adjusted to the direction of the air flow, and the nozzle type is all selected by nozzle 8.

4.3.3. *Spray Dust Fall Device of Negative Pressure in Shifting Operation.* Combining dust migration rules in shifting operation and characteristics of nozzles, the spray dust fall device of negative pressures in shifting operation have been researched, which are shown in Figure 9.

From Figures 5 and 6, in the process of shifting operation, under the action of gravity, air flow, and dust collision, there is not only the transverse diffusion of workplace section but also the longitudinal diffusion to the outlet end under the action of air flow. The trend of diffusion to the rear of the support is greater than that to the coal wall, and respiratory dust accounts for a certain proportion.

The device is mainly composed of two side suction ports (A), one rear suction port (B), and five nozzles (three in the front and one on each side). The three front nozzles (D) are nozzle 5, nozzle 6, and nozzle 5 from top to bottom, and nozzle 6 is selected for side nozzle (C).

After spraying, 3 nozzles at the front and 2 nozzles on the side (1 nozzles on each side) are sprayed to form a fog field, so that the inhaled dust can be fully mixed, coagulated, and settled at the location of the spray port with the fog field. After the nozzle is sprayed, the ejector airflow will be generated, so that the dust will be inhaled from the side suction port and the rear dust collection port. The side dust suction port is rectangular, which is mainly used to inhale the dust generated during frame moving. The rear dust suction port is bell shaped, which can not only absorb the dust generated by the moving frame but also the dust transported to the sidewalk of the hydraulic support.

4.3.4. Application Effect

(1) *Analysis on Dust Reduction Effect of Coal Mining Operation.* The field application effect of the dust fall device with negative pressure in coal mining operation is shown in Figure 10. Dust concentration before and after opening of devices and dust fall rate are shown in Table 10.

(2) *Dust Reduction Effect Analysis of Moving Frame Operation.* The field application effect of the two negative dust fall devices with negative pressure for shifting operation is shown in Figure 11. Dust concentration before and after opening of devices and dust fall rate are shown in Table 11.

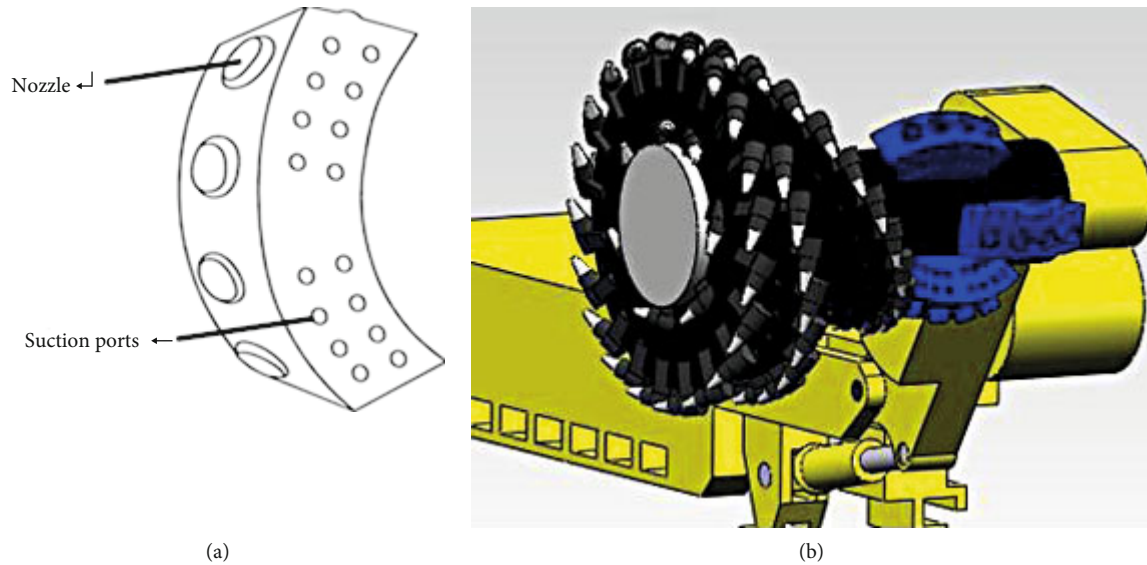
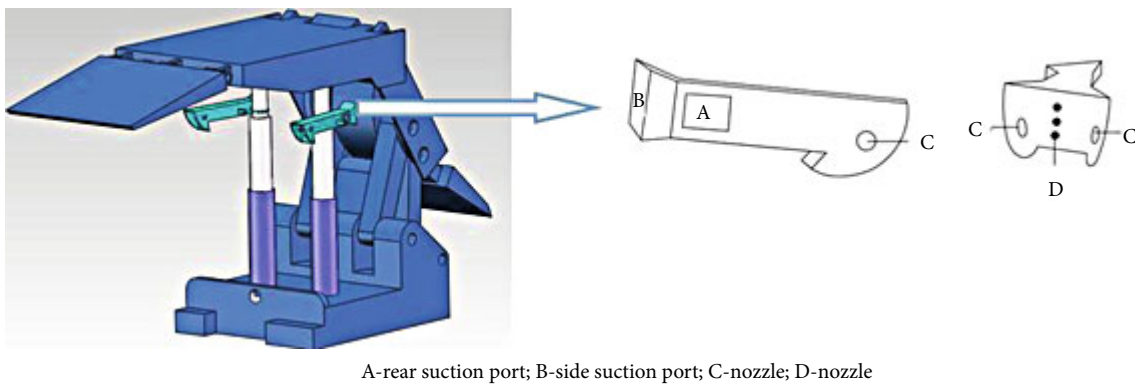


FIGURE 8: Two times dust suppression device for negative pressure in coal mining operation.



A-rear suction port; B-side suction port; C-nozzle; D-nozzle

FIGURE 9: Two times dust suppression device for spraying negative pressure in shifting operation.

5. Analysis and Discussion

5.1. Dust Concentration Changing Regularities in Coal Mining Operation. It can be seen from Figure 3 that due to the limited trend of dust horizontal diffusion, the maximum dust concentration values on the sections 0.2 m, 0.4 m, and 0.6 m away from the coal wall gradually decrease. Due to the effect of ventilation velocity, the maximum dust concentration at the rear drum is greater than that at the front drum. It can be seen from Figure 4 that the dust concentration in the x -axis direction starts to increase under the leading role of inertia at the initial moment and then gradually decreases under the action of ventilation. At the height of 1.5 m away from the ground and at the distance of 0.2 m, 0.4 m, and 0.6 m away from the coal wall, the maximum dust concentration value first increases and then decreases, and the dust concentration reaches the maximum at 0.4 m away from the coal wall.

5.2. Dust Concentration Changing Regularities in Support Shifting Operation. It can be seen from Figure 5 that the dust

generated by the support shifting in the fully mechanized mining face diffuses from the dust source to both sides of the support along the z -axis direction, reaches the maximum concentration near the dust source, and decreases greatly along both sides of the support. The maximum dust concentration at 1 m away from the coal wall is the largest, the maximum dust concentration at the distance of 0.7 m, 1.5 m, and 2 m away from the coal wall is reduced, and the dust concentration at 5 m away from the coal wall is very small.

It can be seen from Figure 6 that the maximum dust concentration at the distance of 0.2 m, 0.7 m, 1 m, 1.5 m, and 2 m away from the coal wall and at the height of 1.5 m above the ground is different. The dust concentration is the lowest at 0.2 m away from the coal wall, increases at the position 0.7 m away from the coal wall, reaches the maximum value at 1.0 m away from the coal wall, and gradually decreases at the position 1.5 m and 2.0 m away. It also can be seen from Figure 6 that the dust concentration starts to produce dust at about $z = 3$, and then, the variation range of dust concentration along the wind direction is not very large at the distance of 0.7 m, 1.5 m, and 2 m away from the coal wall.



FIGURE 10: Field application diagram of negative dust collecting device in coal mining operation.

TABLE 10: Dust concentration before and after opening of devices and dust fall rate.

No.	Dustiness	Total dust concentration (mg/m ³)		Exhaled dust concentration (mg/m ³)		Total dust fall rate	Exhalation rate
		Before opening	After	Before opening	After		
1#	Coal	500	53.1	350	92.7	0.89	0.73
2#	Coal	1100	90.3	500	100.8	0.91	0.79
3#	Coal	1300	113.6	700	140	0.91	0.80
4#	Coal	900	98.7	600	178.2	0.89	0.70
5#	Coal	800	76.2	400	159	0.90	0.60
6#	Coal	400	59.6	200	63.2	0.85	0.68
7#	Coal	220	32.6	100	39.8	0.85	0.60

The dust concentration at 1 m away from the coal wall begins to increase significantly and then changes little. However, the dust concentration at 0.2 m away from the coal wall gradually increases, but the overall concentration is not large. It can be seen that the dust concentration is high near the dust source; the dust not only diffuses to the outlet but also diffuses to the coal wall in the turbulent area.

5.3. Experiment on Atomization Characteristics of Nozzles.

From Table 2, it is can be seen that with the increase of spray pressure, the atomization parameters of nozzles decrease, and the atomization effect is improved in different degrees. Because the mist flow shape of nozzle 2 and nozzle 1 is a sector and the area is small, the dust removal effect is relatively poor in the fully mechanized mining face. Therefore in 8 MPa pressure the atomization effect of nozzle 3-nozzle 8 was studied, which is shown in Tables 7 and 8. According to the droplet particle size data such as $D_{0.1}$, $D_{0.5}$, $D_{0.9}$, D_{32} , D_{43} , and best dust collected particle size of respirable dust,

nozzle 3-nozzle 8 are divided into three categories based on the atomization effect. Nozzle 6 and nozzle 8 belong to the first class and have the best atomizing effect. Nozzle 8's atomization quality indexes have the better comprehensive effect, and the percentage of respirable dust being captured was more than 91%. The atomizing angle of nozzle 8 is greater than that of nozzle. The nozzle range is greater, and the flow is slightly larger. Nozzle 5 and nozzle 7 are the second class and have the second atomization effect. The atomizing angle of nozzle 5 is 75.8 degrees and has the maximum atomizing angle in 8 nozzles. Nozzle 5 has the minimum range of 4.3 m and the smallest flow of 6.67 L/min. But, the percentage of respirable dust being captured is 77.11% and is smaller than that of nozzle 6 and nozzle 8. The nozzle 3 and nozzle 4 are the third kinds of nozzles, and the atomizing effect is the worst.

5.4. Spray Dust Fall Experiment. From Table 9 it is can be seen that the ranking of dust removal is: nozzle 8 > nozzle



FIGURE 11: Field application diagram of dust collecting device in support shifting operation.

TABLE 11: Dust concentration and dust fall rate before and after opening of devices.

No.	Dustiness	Total dust concentration (mg/m ³)		Exhaled dust concentration (mg/m ³)		Total dust fall rate	Exhalation rate
		Before opening	After	Before opening	After		
1#	Coal	360	22.8	160	35.6	0.93	0.77
2#	Coal	500	30.1	200	60.1	0.93	0.70
3#	Coal	480	32.8	210	51.3	0.93	0.75
4#	Coal	400	38.7	190	44.3	0.90	0.76
5#	Coal	320	20.1	180	36.8	0.93	0.79
6#	Coal	200	19.7	130	26.9	0.90	0.79
7#	Coal	130	12.1	80	17.6	0.91	0.78

6 > nozzle 7 > nozzle 5 nozzle 3 > nozzle 4. The total dust and respirable dust reduction rate of nozzle 8 reached 65.82% and 61.70%, respectively, those of nozzle 6 reached 63.56% and 59.78%, respectively, and those of nozzle 5 reached 56.30% and 51.21%, respectively, which are lower than those of nozzle 6 and nozzle 8. Therefore, considering the comprehensive atomization characteristics and spray dust reduction experimental results, as the flow of nozzle 5 is small and the atomizing angle is big, nozzle 5 is suitable when the range is not big and the respirable dust content is small. When the respirable dust content is larger, nozzle 6 and nozzle 8 can be selected. When the desired range is larger than 5 m, nozzle 8 can be selected; otherwise, nozzle 6 can be selected.

5.5. Analysis and Discussion of Spray Dust Fall Effect. From Table 10 and Figure 10, it is known that in 3^{top1110} coal mining face, the total dust concentration and exhaled dust concentration reached the highest value of 1300 mg/m³ and 700 mg/m³, respectively, when the negative pressure dust removal device is not opened. The total dust fall rate was 85% to 91%, and the exhaled dust fall rate was 60% to 80% before and after using the negative dust removal device. The dust concentration in the work face decreased significantly.

From Table 11 and Figure 11, it is known that in 3^{top1110} coal mining face shifting work the highest value of total dust concentration and exhaled dust concentration reached

500 mg/m³ and 200 mg/m³, respectively, when the negative pressure two times dust removal device is not opened. The total dust fall rate was 90% to 93%, and the exhaled dust fall rate was 70% to 79% before and after using the negative dust removal device. The dust concentration in the work face decreased significantly.

6. Conclusions

- (1) The mechanism of dust generation and migration rules in fully mechanized mining face are analyzed. Based on the characteristics of turbulent flow viscous bottom layer and the relevant data of Nicholas experiment, the ventilation velocity distribution formula of the viscous bottom part at the entrance section of fully mechanized mining face is derived: $v_x = \bar{v} \sqrt{2(1 - r/r_0)}$
- (2) The user-defined function of entrance section velocity of the 3^{top1110} fully mechanized coal mining face of Gao Zhuang Coal Mine is compiled by using C language and is set as the boundary condition of entrance speed in FLUENT software. FLUENT software is used to simulate the dust migration law of coal mining and support shifting operations under different conditions
- (3) Based on the experiment of spray and dust fall of nozzles in the 3^{top1110} fully mechanized coal mining face of Gao Zhuang Coal Mine, 3 kinds of nozzles with better dust reduction effect were selected. Among them, nozzle 5 had a smaller flow rate and larger atomization angle and had little requirement for range. Nozzle 5 could be selected for the smaller respirable dust content. For the larger respirable dust content, nozzle 6 and nozzle 8 could be selected. When the range requirement was greater than 5 m, choose nozzle 8; otherwise, choose nozzle 6
- (4) According to the law of dust movement in the 3^{top1110} fully mechanized mining face and the characteristics of nozzles, two spray dust reduction devices of negative pressure in the fully mechanized mining face of Gao Zhuang Coal Mine were studied. By using the negative pressure dust fall device, in the coal mining operation, the total dust fall rate was 85% to 91% and the exhaled dust fall rate was 60% to 80%. And in the support shifting operation, the total dust fall rate was 90% to 93% and the exhaled dust fall rate was 70% to 79%.

Data Availability

The raw/processed data required to reproduce these findings cannot be shared at this time as the data also forms part of an ongoing study.

Conflicts of Interest

The authors declare that they have no conflicts of interest.

Acknowledgments

The authors thank the help of Professor Gang Zhou and Professor Wen Nie in the experiment of spray dust fall. The research was sponsored by the Key research and development plan of Shandong Province (Project No. 2017GSF220016).

References

- [1] H. M. Yu, W. M. Cheng, L. R. Wu, H. Wang, and Y. Xie, "Mechanisms of dust diffuse pollution under forced-exhaust ventilation in fully-mechanized excavation faces by CFD-DEM," *Powder Technology*, vol. 317, pp. 31–47, 2017.
- [2] G. B. Zhang, B. Sun, S. Z. Song, H. Wang, and G. Zhou, "CFD comparative analysis on the pollution characteristics of coal dust under turbulent airflow from coal cutting in the fully mechanized mining face," *Process Safety and Environmental Protection*, vol. 146, pp. 515–530, 2021.
- [3] Y. S. Lai, *Study on dust distribution law and computer simulation of fully mechanized working face*, China University of mining and technology, 1995.
- [4] S. Nakayama, K. Uchino, and M. Inoue, "Three dimensional flow measurement at heading face and application of CFD," *Shigen-To-Sozai*, vol. 112, pp. 639–644, 1996.
- [5] N. A. Patankar and D. D. Joseph, "Modeling and numerical simulation of particulate flows by the Eulerian- Lagrangian approach," *International Journal of Multiphase Flow*, vol. 27, no. 10, pp. 1659–1684, 2001.
- [6] M. Z. Yu, H. H. Jin, L. H. Chen, J. H. Fan, and K. F. Cen, "Cen. large eddy simulation study on the movement and diffusion characteristics of dust particles," *Journal of Environmental Science*, vol. 25, pp. 891–895, 2005.
- [7] C. Housiadas, Y. Drossinos, and M. Lazaridis, "Effect of small-scale turbulent fluctuations on rates of particle formation," *Journal of Aerosol Science*, vol. 35, no. 5, pp. 545–559, 2004.
- [8] X. Z. Wang, Z. A. Jiang, S. Wang, and Y. Liu, "Numerical simulation of dust concentration distribution in coal roadway driving process," *Journal of China Coal Society*, vol. 32, pp. 386–390, 2007.
- [9] Y. Liu, Z. A. Jiang, W. Cai, F. Z. Zhou, D. Guo, and B. D. Liu, "Numerical simulation of the dust movement rule in fully-mechanized coal faces," *Journal of University of Science and Technology Beijing*, vol. 29, pp. 351–353, 2007.
- [10] W. Niu, Z. A. Jiang, and Y. Liu, "Numerical simulation on dust movement regularities at fully-mechanized coal faces and its utilization," *Journal of Liaoning Technical University, Natural Science*, vol. 29, pp. 357–360, 2010.
- [11] Z. Gang, *Research of theory about dust prevention by water-cloud and relevant techniques for fully-mechanized caving coal face*, Shandong University of Science and Technology, 2009.
- [12] G. Zhou, W. M. Cheng, L. J. Chen, and W. Nie, "Numerical simulation and application of dust concentration spatial distribution in fully mechanized top coal caving face," *Journal of China Coal Society*, vol. 35, pp. 2094–2099, 2010.
- [13] L. R. Wu, *Study on dust movement rule of fully mechanized top coal caving working face and two times dust suppression device with spray negative pressure*, Beijing University of science and technology, 2014.
- [14] B. Sun, W. M. Cheng, H. Wang, and J. Y. Wang, "Influence of rotary flow wind of drum in fully mechanized mining face on

- lateral dispersion law of coal dust in cutting,” *Journal of China Coal Society*, vol. 8, pp. 2269–2279, 2018.
- [15] X. W. Yao, G. L. Lu, and K. L. Xu, “Numerical simulation of dust generation at different procedures in steeply inclined fully-mechanized caving face,” *Journal of China Coal Society*, vol. 40, pp. 389–396, 2015.
- [16] T. Ren, Z. Wang, and J. Zhang, “Improved dust management at a longwall top coal caving (LTCC) face - A CFD modelling approach,” *Advanced Powder Technology*, vol. 29, no. 10, pp. 2368–2379, 2018.
- [17] C. Hankwon, P. H. Jin, and D. J. Hee, “Flame synthesis of silica nanoparticles by adopting two-fluid nozzle spray,” *Colloids and Surfaces A: Physicochemical and Engineering Aspects*, vol. 1, pp. 140–144, 2008.
- [18] N. I. Jayaraman and R. A. Jankowski, “Atomization of water sprays for quartz dust control,” *Applied Industrial Hygiene*, vol. 3, no. 12, pp. 327–331, 1988.
- [19] L. J. Goldbeck and A. D. Marti, “Dust control at conveyor transfer points: containment, suppression and collection,” *Bulk Solids Handling*, vol. 16, pp. 367–372, 1996.
- [20] W. M. Cheng, W. Nie, G. Zhou, and Q. M. Zuo, “Study on dust reduction performance of high pressure spray atomization particle size in coal mine,” *Journal of China University of Mining and Technology*, vol. 40, pp. 185–189, 2011.
- [21] Z. C. Liu, “Theoretical analysis and experimental study on fire extinguishing of straight through swirl water mist nozzle,” *Sichuan, Southwest Jiaotong University*, 2008.
- [22] X. Q. Wang, J. Qin, and Z. W. Xie, “Application of three dimensional LDV/APV system in measurement of characteristic parameters of dust nozzle,” *Journal of China Coal Society*, vol. 35, pp. 269–272, 2010.
- [23] G. Zhou, W. Nie, and W. M. Cheng, “Analysis of influence of high pressure atomization dust suppression on micro parameters of dust particles in fully mechanized top coal caving face,” *Journal of China Coal Society*, vol. 39, pp. 2053–2059, 2014.
- [24] H. T. Peng, W. Nie, H. M. Yu et al., “Research on mine dust suppression by spraying: development of an air-assisted PM10 control device based on CFD technology,” *Advanced Powder Technology*, vol. 30, no. 11, pp. 2588–2599, 2019.
- [25] P. F. Wang, R. H. Liu, M. Tang, W. Zhang, and Z. Gui, “Experimental study on atomization characteristics and dust suppression efficiency of high-pressure spray in underground coal mine,” *Journal of China Coal Society*, vol. 40, pp. 2124–2130, 2015.
- [26] P. F. Wang, H. Han, C. Tian, R. Liu, and Y. Jiang, “Experimental study on dust reduction via spraying using surfactant solution,” *Atmospheric Pollution Research*, vol. 11, no. 6, pp. 32–42, 2020.
- [27] Y. Yu, “Investigations into roadway air velocity distribution,” *Journal of Huainan Mining Institute*, vol. 1, pp. 17–24, 1989.